Model-independent measurement of the CKM angle γ through $B^{\pm} \to D^0 K^{\pm}$ decays with LHCb and CLEO-c

Claire Prouve

Third year report

Presented to the
School of Physics
of the
University of Bristol

29 May 2016

Contents

Analysis part

1.1 Introduction

The work done in the first part of the second year of this phd program consisted of a determination of the CP-even fraction of the decay of the D meson into 4 pions. The CP-even fraction of the decay was determined using correlated D meson pairs produced at the lepton collider CESR and reconstructed by the CLEO-c detector. The results of this analysis have been published are now used by the Oxford group to measure the CKM gamma angle using LHCb data.
The last month of work was used towards producing an alignment for the RICH detectors in the LHCb experiment for RunII.

Unless otherwise stated all activities described in this report were performed by the author.

1.2 Determining the CP-even fraction of $D \to 4\pi$

1.2.1 Short theory

The simplest way of determining the CP-even fraction of a decay using correlated pairs is by measuring the rate of events against decays with definitive CP-eigenstates. This part of the analysis was performed by the Oxford group.
Another way of determining the CP-even fraction is by reconstructing it against a decay which strong phase difference in different bins of phasespace has been determined previously. The decay used here is $D \to K^0_S\pi\pi$ and $D \to K^0_L\pi\pi$.
The CP-even fraction $F^{4\pi}_+$ of 4π can be determined through the evaluation of

$$M_i^{K^0_S\pi\pi} = h_{K^0_S\pi\pi}(T_i^{K^0_S\pi\pi} + T_{-i}^{K^0_S\pi\pi} - 2\,c_i\sqrt{T_i^{K^0_S\pi\pi}T_{-i}^{K^0_S\pi\pi}}\,(2F_+^{4\pi} - 1)) \tag{1.1}$$

and

$$M_i^{K^0_L\pi\pi} = h_{K^0_L\pi\pi}(T_i^{K^0_L\pi\pi} + T_{-i}^{K^0_L\pi\pi} + 2\,c'_i\sqrt{T_i^{K^0_L\pi\pi}T_{-i}^{K^0_L\pi\pi}}\,(2F_+^{4\pi} - 1)) \tag{1.2}$$

where the M_i denote the number of events in bin i of the $K^0_S\pi\pi$/ $K^0_L\pi\pi$ Dalitz-Plot tagged against 4π, the T_i the relative amount of events in bin i of flavour-tagged $K^0_S\pi\pi$/ $K^0_L\pi\pi$ Dalitz-Plot and the h are normalisation factors.
By summing over the bins i and $-i$ these expressions become

$$MM_i^{K^0_S\pi\pi} = M_i^{K^0_S\pi\pi} + M_i^{K^0_S\pi\pi} = 2\cdot h_{K^0_S\pi\pi}(T_i^{K^0_S\pi\pi} + T_{-i}^{K^0_S\pi\pi} - 2\,c_i\sqrt{T_i^{K^0_S\pi\pi}T_{-i}^{K^0_S\pi\pi}}\,(2F_+^{4\pi} - 1)) \tag{1.3}$$

and

$$MM_i^{K^0_{\rm L}\pi\pi} = M_i^{K^0_{\rm L}\pi\pi} + M_{-i}^{K^0_{\rm L}\pi\pi} = 2 \cdot h_{K^0_{\rm L}\pi\pi}(T_i^{K^0_{\rm L}\pi\pi} + T_{-i}^{K^0_{\rm L}\pi\pi} + 2\, c_i' \sqrt{T_i^{K^0_{\rm L}\pi\pi} T_{-i}^{K^0_{\rm L}\pi\pi}}\, (2F_+^{4\pi} - 1)) \tag{1.4}$$

The following report summarised how the values for $MM_i^{K^0_{\rm S}\pi\pi}$ and $MM_i^{K^0_{\rm L}\pi\pi}$ are determined.

1.2.2 Binned $K^0_{\rm S}\pi\pi$/ $K^0_{\rm L}\pi\pi$ vs 4π yields

The values for $MM_i(K^0_{\rm S}\pi\pi)$ are obtained by counting the number of $K^0_{\rm S}\pi\pi$/ $K^0_{\rm L}\pi\pi$ vs. 4π events, subtracting the bkg in the sample and then correcting for different signal reconstruction and selection efficiencies in the different bins of the $K^0_{\rm S}\pi\pi$/ $K^0_{\rm L}\pi\pi$ Dalitz-Plot. The contributions to the yields for the $K^0_{\rm S}\pi\pi$ tag are listed below:

$$MM_i^{K^0_{\rm S}\pi\pi} = (N_i^{meas} - B_i^{peak} - B_i^{flat})/\epsilon_i \tag{1.5}$$

- $MM_i^{K^0_{\rm S}\pi\pi}$: absolute number of 4π vs $K^0_{\rm S}\pi\pi$ events in bin i. This is the quantity that enters the fit for F_+.

- N_i^{meas} : total number of reconstructed and selected events in bin i.

- B_i^{peak} : number of reconstructed and selected peaking bkg. events in bin i. The only peaking bkg. expected is $K^0_{\rm S}\pi\pi$ vs $K^0_{\rm S}\pi\pi$ where on of the $K^0_{\rm S}\pi\pi$ decays is reconstructed as a 4π.

- B_i^{flat} : number of reconstructed and selected flat bkg. events in bin i.

- ϵ_i : reconstruction and selection efficiency for 4π vs $K^0_{\rm S}\pi\pi$ events in bin i.

The values for $MM_i^{K^0_{\rm L}\pi\pi}$ are obtained using:

$$MM_i^{K^0_{\rm L}\pi\pi} = (N_i^{meas} - B_i^{peak} - B_i^{flat} - B_i^{cont})/\epsilon_i \tag{1.6}$$

- $MM_i^{K^0_{\rm L}\pi\pi}$: absolute number of 4π vs $K^0_{\rm L}\pi\pi$ events in bin i. This is the quantity that enters the fit for F_+.

- N_i^{meas} : total number of reconstructed and selected events in bin i.

- B_i^{peak} : number of reconstructed and selected peaking bkg. events in bin i. The two peaking bkgs considered in this case are $K^0_{\rm L}\pi\pi$ vs $K^0_{\rm S}\pi\pi$ where the $K^0_{\rm S}\pi\pi$ is reconstructed as 4π (8% of the events in the signal window) and $K^0_{\rm S}\pi\pi$ vs 4π where the $K^0_{\rm S}$ is not reconstructed (1.9% of the events in the signal window).

- B_i^{flat} : number of reconstructed and selected flat bkg. events in bin i.
- B_i^{cont} : number of reconstructed and selected continuum bkg. events in bin i.
- ϵ_i : reconstruction and selection efficiency for 4π vs $K^0_L\pi\pi$ events in bin i.

The contributions for the $K^0_L\pi\pi$ tag have another component, which is the continuum bkg. This bkg does not appear in the $K^0_S\pi\pi$ tag because in this tag requires 4 pions to be reconstructed while in the $K^0_L\pi\pi$ case only 2 pions are reconstructed.
The distribution of reconstructed $K^0_S\pi\pi$/ $K^0_L\pi\pi$ vs 4π events in the phasespace of the tag can be seen in Figure 1.1.

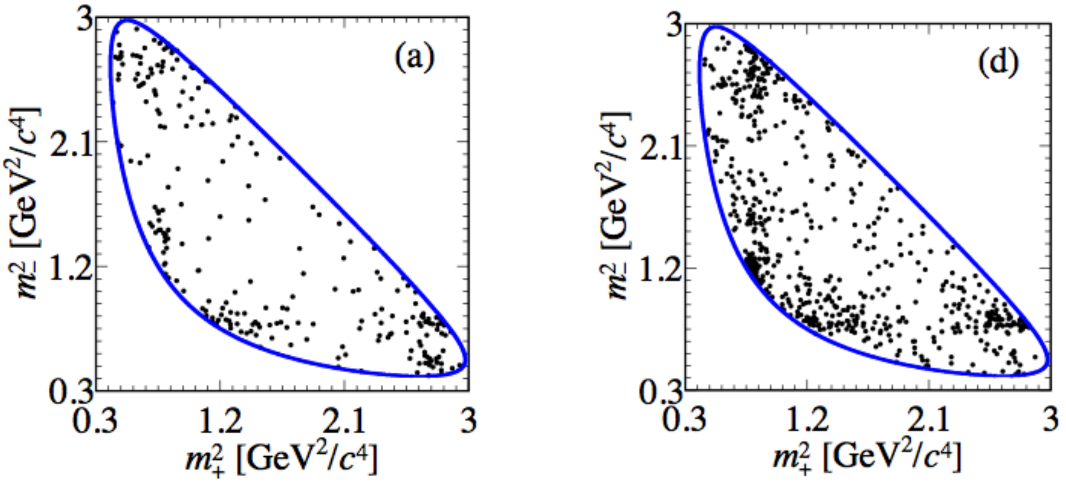

Figure 1.1: *Dalitz-plot distributions for $K^0_S\pi\pi$ (left) and $K^0_L\pi\pi$ (right) reconstructed against 4i.*

1.2.2.1 Determination of number of flat and continuum background events

The total number of flat bkg events is determined using a combination of sidebands and extrapolated to the signal region. As the name suggest, the flat background is distributed evenly over the $K^0_S\pi\pi$ phasespace. Therefore the distribution across the different $K^0_S\pi\pi$ bins is used according to the area of each bin.
The same is true for the continuum bkg, only that the total number of continuum bkg events was determined using the continuum MC sample produced by CLEO-c and scaling according to the luminosity of the data sample.

1.2.2.2 Determination of peaking bkg events

The total number of peaking bkg events was determined by scaling their contribution in the generic MC sample to the data sample. The distribution of those events over the bins of the $K^0_S\pi\pi$/ $K^0_L\pi\pi$ phasespace was determined using a combination of data-driven and MC-driven techniques.

1.2.2.3 Determination of the signal efficiency

The signal efficiency of both the $K^0_S\pi\pi$ and the $K^0_L\pi\pi$ tags were determined using a signal MC sample of 250k events.

1.2.3 Fit for $F_+(4\pi)$

1.2.3.1 Input from former analyses

The given values for K'_i obtained from Table 1 of `arXiv:1210.939` contain effects from charm-mixing that cancel in our case. The factors T_i without mixing are archived by numerically solving the system of equations:

$$K'_i = T_i + \sqrt{T_i T_{-i}}(yc_i + xs_i) \tag{1.7}$$

where x and y charm-mixing parameters. The fit also takes into account that the sum over the T_i should be one by fixing $T_1 = 1 - \sum_{i\neq 1} T_i$. The values for x and y are take from the latest HFAG results ($x = (0.63 \pm 0.19)\%$, $y = (0.75 \pm 0.12)\%$) and the values for c_i and s_i are taken from `arXiv:1010.2817`. In the fit all input variables are Gaussian constraint and the correlation between c_i and s_i are taken into account.

The fractional flavour-tagged $K^0_L\pi\pi$ yields are taken from Sean Brisbane's thesis (Section 3., Table 3.14).

1.2.3.2 Results F_+

A fit for F_+ is performed for the default signal results, for the results with stat. error only.
In order to determine the effect of the systematic uncertainties - most of which come for the estimation of bkg events - the each systematic uncertainty is separately added to the statistic uncertainty and the fit is performed again.
Listing the statistical error and the systematic error from the Dalitz plot acceptance separately this results in $F_+ = 0.737 \pm 0.049 \pm 0.024$ where the first error is statistical and the second one systematic. These results are in very good agreement with the result from the CP-eigenstate analysis which yielded a value of $F_+ = 0.754 \pm 0.031 \pm 0.021$.

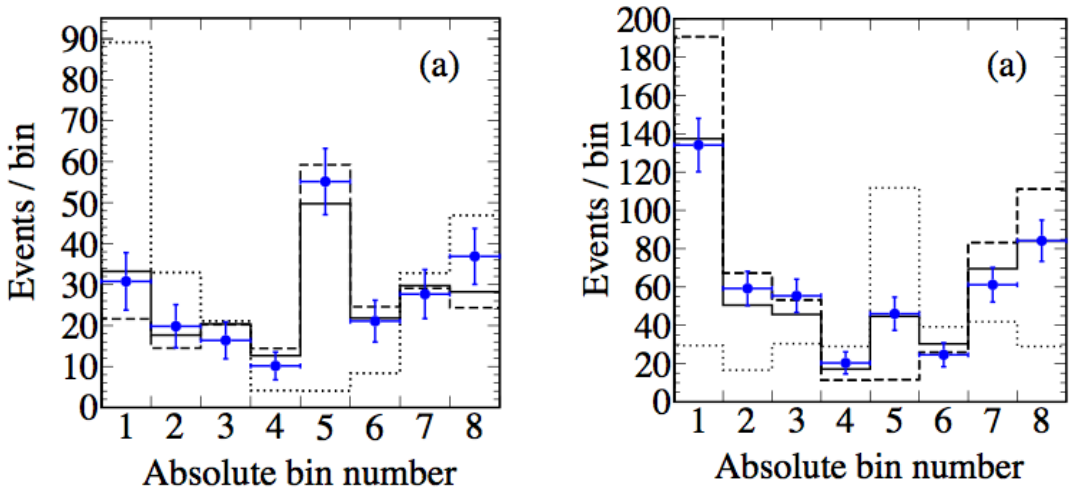

Figure 1.2: *Distribution of signal yields per bin for $K^0_S\pi\pi$ (left) and $K^0_L\pi\pi$ (right). Red: data, solid line: fit results, dotted line: values for F_+=0, dashed line: values for F_+=1.0.*

2. RichAlignment

This is an extract from the public note I am writing about the new RICH mirror alignment procedure for Run II of the LHC.

2.1 Introduction

The LHCb experiment uses two ring-imaging Cherenkov (RICH) detectors to provide powerful discrimination between charged particles in the intense hadron production environment of the LHC. These two separate RICH detectors have different radiators and are designed to provide particle identification over a momentum range of 1 to 100 GeV/c [1]. The performance of the particle identification supplied by the RICH system [2] strongly depends on the quality of its alignment, i.e. how accurately the physical position of each component of the RICH detectors is described in the LHCb software. The goal of the alignment procedure is determine the exact position of all optical components and propagate this information to the LHCb conditions database that stores the non-event time-varying data pertaining to detector conditions. The LHCb detector achieved excellent performance in Run I but faces more challenging conditions in Run II. The LHC will collide protons at an increased centre-of-mass energy of 13 TeV and with 25 ns bunch spacing. The spatial alignment of the detector and the accurate calibration of its subcomponents are essential to achieve the best physics performance. In order to keep the selection efficiencies in the high level trigger as high as in Run I, conditions on the particle identification will be used in Run II. This requires the full alignment and calibration of the RICH detectors within the high performance trigger sequence.
This note describes how the LHCb RICH optical systems are aligned in software in Run II using proton-proton collision data. The method used is discussed in Section 2.3, while the computing framework and the implementation for the automated running of the alignment is described in Section 2.4. The results for the data-taking period in 2015 are presented in Section **??**.

$$O = \frac{\sum^{ADC>thresh.} N_{events}}{\sum N_{events}} \tag{2.1}$$

2.2 The LHCb detector

The LHCb detector [1,3] is a single-arm forward spectrometer covering the pseudorapidity range $2 < \eta < 5$, designed for the study of particles containing b or c quarks. The

detector includes a high-precision tracking system consisting of a silicon-strip vertex detector surrounding the pp interaction region, a large-area silicon-strip detector located upstream of a dipole magnet with a bending power of about 4 Tm, and three stations of silicon-strip detectors and straw drift tubes placed downstream of the magnet. The tracking system provides a measurement of momentum, p, of charged particles with a relative uncertainty that varies from 0.5% at low momentum to 1.0% at 200 GeV/c. The minimum distance of a track to a primary vertex, the impact parameter, is measured with a resolution of $(15 + 29/p_{\mathrm{T}})\,\mu$m, where p_{T} is the component of the momentum transverse to the beam, in GeV/c.
Different types of charged hadrons are distinguished using information from two ring-imaging Cherenkov detectors [2]. Photons, electrons and hadrons are identified by a calorimeter system consisting of scintillating-pad and preshower detectors, an electromagnetic calorimeter and a hadronic calorimeter. Muons are identified by a system composed of alternating layers of iron and multiwire proportional chambers.
The event selection is performed by a trigger, which consists of a hardware stage, based on information from the calorimeter and muon systems, followed by a software stage, which applies a full event reconstruction.
In Run II, the alignment and calibration of all subdetectors is performed online in between different stages of the high level trigger (HLT) and the results are immediately applied to the reconstruction.

2.2.1 RICH optical systems

Both RICH1 and RICH2 have two sets of mirrors: the primary spherical mirrors, and the secondary (a.k.a. plane, flat), much flatter mirrors. Cherenkov photons emitted by a charged track are reflected off a primary mirror onto a secondary mirror, and from there out of the LHCb acceptance onto the plane of photon detectors, which coincides with the focal plane of the given part of the optical systems. The RICH1/RICH2 optical systems consists of 4/56 primary and 16/40 secondary mirrors. The layouts of the RICH optical systems are shown in Figure 2.1 [4, 5], while the structures of the mirror arrays and their numbering are shown in Figures **??** and **??** of Section 2.3.

The right-handed coordinate system of each mirror segment is defined by placing the origin at the centre of curvature with the x-axis pointing towards the mirror, the y-axis pointing upwards and the corresponding z-axis being horizontal. Finally, the pivot point for the software rotations around the y- and z-axes is at the centre of each mirror.
In order to achieve the optimal performance of the LHCb RICH detector we aim to minimize the uncertainty, σ, associated with the measurement of a single photon Cherenkov angle. This is limited by four main sources of uncertainty outlined in Table 2.1. Adding them in quadrature gives the minimal total uncertainty, which can be obtained by having an optimal alignment of all optical components of the RICH detectors.

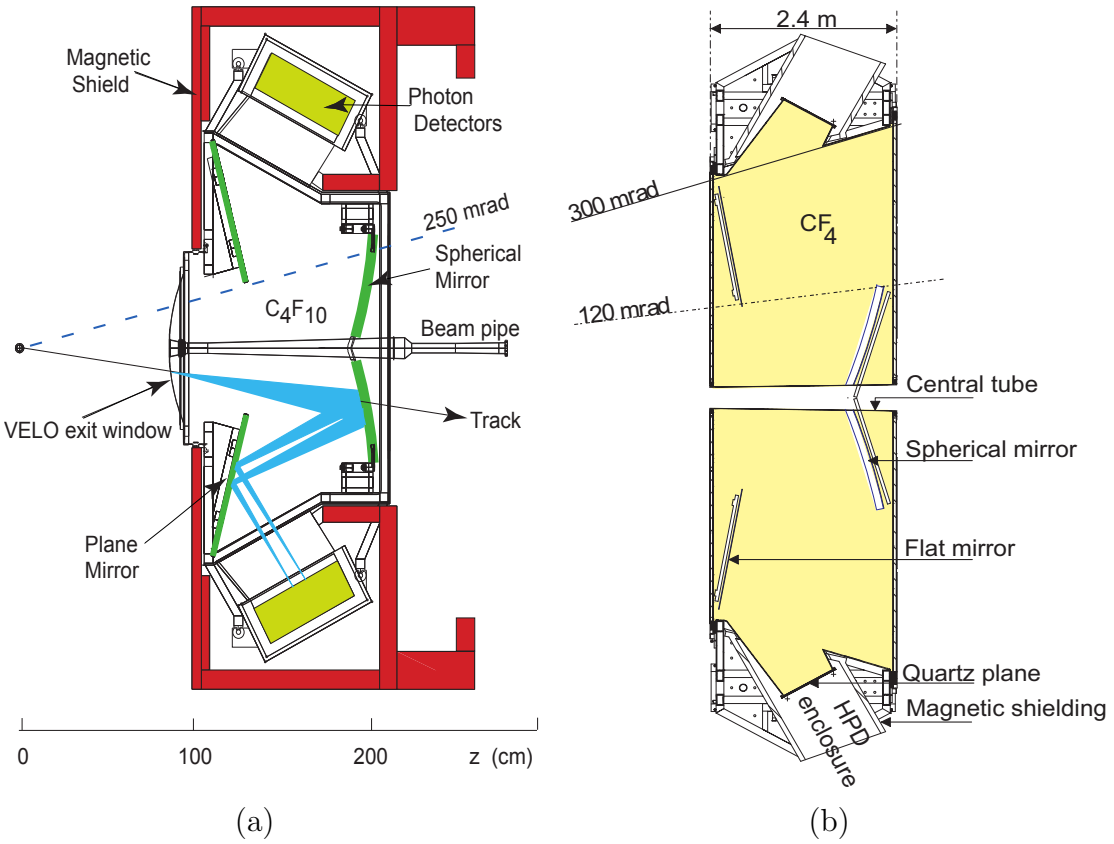

(a) (b)

Figure 2.1: Schematic view of the LHCb RICH detectors and their optical systems: (a) side view of RICH1 and (b) top view of RICH2. Formation of a Cherenkov ring in the lower part of RICH1 is also drawn.

Table 2.1: Sources of uncertainty, σ, of the measurement of a single photon Cherenkov angle for the three LHCb RICH radiators.

	σ [mrad]	
	RICH1	RICH2
	C_4F_{10}	CF_4
Emission point	0.8	0.2
Chromatic dispersion	0.9	0.5
Pixel size	0.6	0.2
Tracking	0.4	0.4
Total	1.5	0.7

2.3 Method of alignment for the RICH optical system

An iterative, data-driven method for finding appropriate software compensations for the mirror misalignments was developed in the HERAb experiment [6]. The approach presented here builds on that method and is developed further to address the more complex design of the LHCb RICH system.

A misalignment in the LHCb RICH optical system manifests itself as a displacement of the observed Cherenkov ring against the expected one [7, 8] as can be seen in

Figure 2.2. This can also be viewed as a discrepancy between the actual center of the Cherenkov ring - e.g. the center of the Cherenkov ring observed on the detector plane - and its expected position calculated from the projection of the track onto the detector plane using the orientation of the optical components given in the current LHCb conditions database.

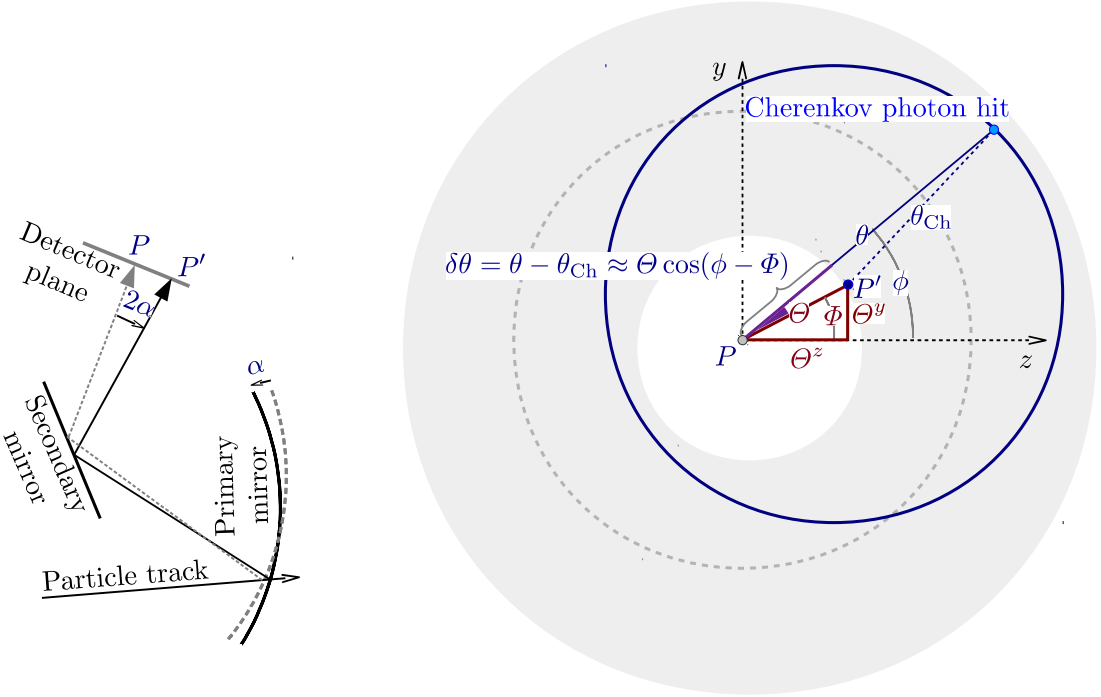

(a) (b)

Figure 2.2: (a) Schematic drawing of how a rotational misalignment of a RICH mirror (primary mirror in this example) causes shift of the actual centre P' of the Cherenkov ring to P on the photon detector plane. The projection of the track is drawn for explanatory purpose and represents the position of the expected centre of the Cherekov ring. (b) The expected Cherenkov angle θ_{Ch} and the reconstructed Cherenkov angle θ are displayed. P marks the position of the extrapolated track projection calculated without adjustments that would compensate any misalignments of the RICH mirrors, while P' is the actual position of the centre of the ring and displaced by Θ^z and Θ^y with respect to P' . Cherenkov angles θ are evaluated relative to P, and therefore, vary with ϕ. The gray stripe represents area around the expected ring from which the photon hits are reconstructed. The width of this stripe is empirically chosen wide enough to cover the actual shifted (and somewhat smeared) ring of hits from a given track. Inevitably, the "noise" background photon hits in this area are also "reconstructed".

In order to observe and quantify the misalignment the quantity $\delta\theta$

$$\delta\theta\left(\phi\right) = \theta\left(\phi\right) - \theta_{\mathrm{Ch}}, \tag{2.2}$$

– where $\theta\left(\phi\right)$ is the the measured Cherenkov angle and θ_{Ch} the expected Cherenkov angle – is plotted against the azimuthal angle ϕ (see Figure 2.2). For perfectly

aligned mirrors $\delta\theta$ is independent of ϕ but in case of a misalignment the distribution is approximately sinusoidal in ϕ

$$\begin{aligned}\delta\theta_{p,s}(\phi) &\equiv [\theta(\phi) - \theta_{\mathrm{Ch}}]_{p,s} \approx [\Theta\cos(\phi - \Phi)]_{p,s} \\ &= [\Theta\cos\Phi\cos\phi + \Theta\sin\Phi\sin\phi]_{p,s} \\ &= \Theta^z_{p,s}\cos\phi + \Theta^y_{p,s}\sin\phi\end{aligned} \tag{2.3}$$

where the factors $\Theta^y_{p,s}$ and $\Theta^z_{p,s}$ represent the misalignments on the detector plane in y and z for a given mirror combination with primary mirror p and secondary mirror s.
The misalignment factors $\Theta^y_{p,s}$ and $\Theta^z_{p,s}$ relate to the individual misalignments of the primary and secondary mirror via the *magnification factors*

$$\begin{aligned}A^y_{p,s}\alpha^y_p + B^y_{p,s}\beta^y_s + a^y_{p,s}\alpha^z_p + b^y_{p,s}\beta^z_s &= \Theta^y_{p,s} \\ A^z_{p,s}\alpha^z_p + B^z_{p,s}\beta^z_s + a^z_{p,s}\alpha^y_p + b^z_{p,s}\beta^y_s &= \Theta^z_{p,s}\end{aligned} \tag{2.4}$$

where α^y_p, α^z_p, β^y_s and β^z_s are the actual tilts of the primary and secondary mirrors around the y- and z-axis with respect to a given database. The magnification factors $A^y_{p,s}$, $B^y_{p,s}$, $a^y_{p,s}$ and $b^y_{p,s}$ ($A^z_{p,s}$, $B^z_{p,s}$, $a^z_{p,s}$ and $b^z_{p,s}$ for the z-axis) translate the effect of a tilt of the mirrors onto the detector plane (see Section 2.3.3).
After all individual mirror tilts have been calculated a new database with the mirror orientations is created. It is useful to apply the alignment procedure iteratively to the same data sample, each time with the new database produced by the previous alignment. The alignment procedure is considered to have converged after no mirror has been found to have a misalignment greater than a chosen convergence criteria.
An overview of the entire alignment procedure can be seen in Figure 2.3 while different details of the procedure are explained in the sections below.

2.3.1 Track and photon selection

The events that the tracks and their photons are taken from are preselected. More information about the preselection and its implementation is given in Section 2.4.
In order to most accurately predict the Cherenkov angle for a given track some selection criteria are applied to the tracks themselves and to the photon candidates that make it into the $\delta\theta$ vs. ϕ histograms.
High-momentum tracks are selected where the assumption can be made that the Cherenkov angle is saturated and therefore does not depend on the particle type any more. Figure 2.4 and Equation 2.3 show the dependency of the Cherenkov angle of the momentum p for different types of particles with mass m in a radiator with refractive index η.

$$\theta_{\mathrm{Ch}} = \arccos\left(\frac{1}{\eta}\sqrt{\left(\frac{m}{p}\right)^2 + 1}\right) \tag{2.5}$$

In the case of high energy tracks all particles are assumed to have the the mass of a pion and the expected Cherenkov angle is calculated under that hypothesis.
The photon hits chosen to fill the $\delta\theta$ vs. ϕ histograms are chosen from a ring-shaped

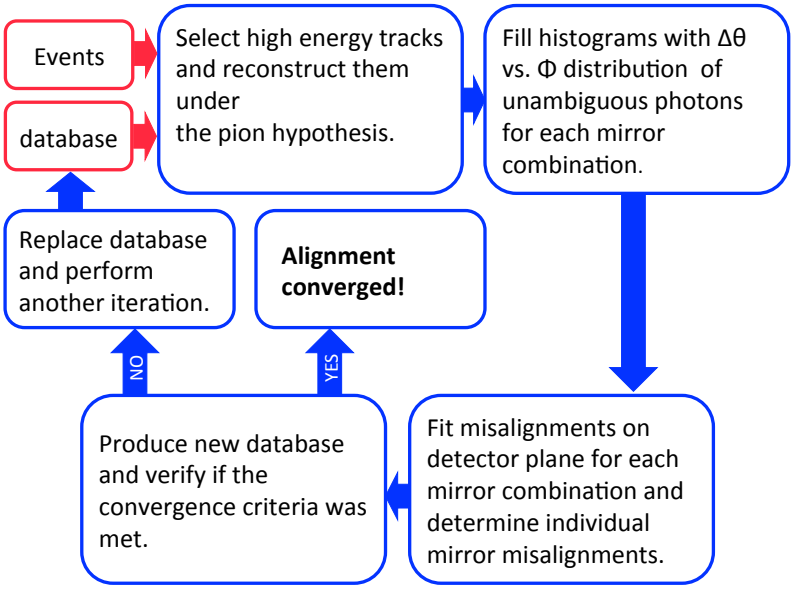

Figure 2.3: Overview of the entire alignment procedure. The alignment starts from a sample of events and usually from the mirror orientation given in the LHCb conditions database. From there high energy tracks are reconstructed under the pion hypothesis (see Section 2.3.1). Then the $\delta\theta$ vs. ϕ histograms are filled for each mirror combination selected for the alignment procedure (see Section 2.3.4) and fitted to get the misalignments on the detector plane. With these the individual mirror misalignments are determined and a new database containing the corrected mirror orientations is created. If the convergence criteria is reached the alignment procedure is finished, if the criteria has not been reached the newly made database is used for the reconstruction of the same events and the entire procedure is repeated.

area around the expected center of the Cherenkov ring (see Figure 2.2). The ring's width is chosen to be big enough to cover the area of a shifted Cherenkov ring from a potentially misaligned mirror combination.
In the calculation of $\delta\theta$ for the histograms the value for $\theta\,(\phi)$ is needed. This value is obtained by matching a photon hit on the detector plane to a track and calculating the Cherenkov angle. This requires an assumption about where along the track the Cherenkov photon was emitted. Since this is a intrinsically unknown quantity the assumption is made that the photon was emitted in the middle of the track. This introduces a source of noise from photons falsely associated with a given track. An analysis of MC events has shown [6] that it is possible to reduce this noise by only reconstructing *unambiguous* photon hits. A photon hit is *unambiguous* if it will be reflected by the same primary and secondary mirror independently of where along the particle track it was emitted. Therefore only unambiguous photon hits are chosen to be used in the alignment procedure in the $\delta\theta$ vs. ϕ histograms.

2.3.2 Method for fitting the $\delta\theta$ vs. ϕ distributions

For every chosen combination of primary mirror p and secondary mirror s, $\delta\theta$ is plotted against ϕ. Each of these two-dimensional distributions is divided into 20 bins in ϕ. Inside each ϕ bin the $\delta\theta$ distribution is fitted with a Gaussian plus a second order polynomial that represents the background photons. In accordance

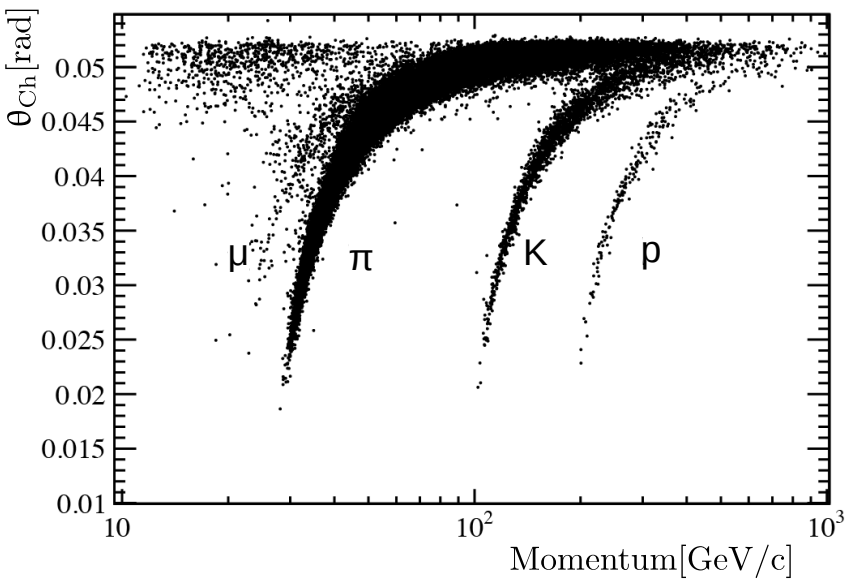

Figure 2.4: Cherenkov angle θ_{Ch} against track momentum, for tracks traversing the RICH1 gaseous radiator. Muons, pions, kaons and protons are visible. As the track momentum increases, all particles tend towards the same θ_{Ch}, known as the saturated Cherenkov angle.

with Equation 2.3 the ϕ dependence of the position of the Gaussian peak for a given mirror combination (p, s) is approximated by

$$\delta\theta_{p,s}(\phi) = \Theta^{z}_{p,s} \cos\phi + \Theta^{y}_{p,s} \sin\phi. \tag{2.6}$$

Equation 2.6 is used as a bond when fitting all the 20 slices jointly.
The fitting is done by means of the ROOT framework [9], in particular, using the MINUIT minimization package. An example of a $\delta\theta$ vs. ϕ histogram for a specific mirror combination in RICH1, including the fitted sinusoidal of Equation 2.6 is shown in Figure 2.5, before alignment and after the alignment.

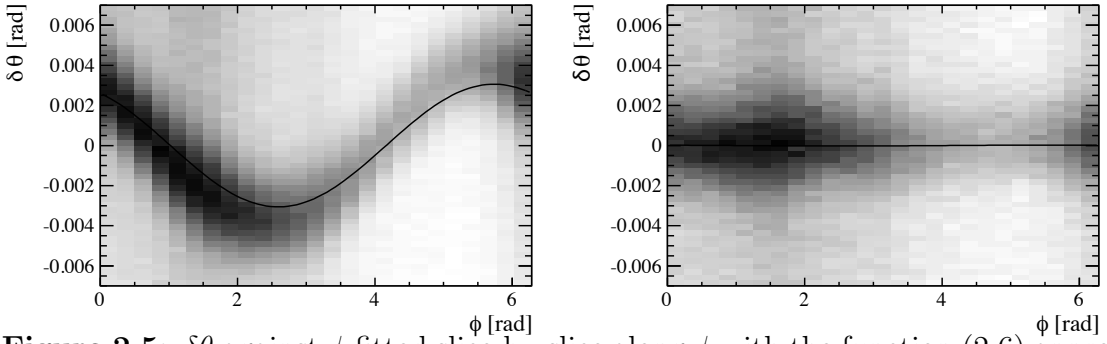

Figure 2.5: $\delta\theta$ against ϕ fitted slice-by-slice along ϕ with the function (2.6) approximating the position of the Gaussian peaks on the ϕ-$\delta\theta$ plane for the combination of primary mirror 0 and secondary mirror 1 of the RICH1. The originally misaligned mirror combination is represented on the left while the right plot shows the same mirror combination after the alignment procedure.

2.3.3 Magnification factors

The magnification factors relate the tilts of the individual mirrors to the misalignment that can be observed in the detector plane. The effect of the magnification

factors can be demonstrated in a simplified manner by considering small rotations of primary and secondary mirrors around their y- axes. Those small rotations yield approximately the following displacement of the observable Cherenkov ring (as shown in Fig. 2.2):

$$l\,\Theta^y \approx l_{\text{pri}} 2\,\alpha^y - l_{\text{sec}} 2\,\beta^y, \tag{2.7}$$

where l, l_{pri} and l_{sec} are lengths' of the paths of the photons to the photon detectors (from the emission point, from the primary mirror, and from the secondary mirror, respectively). Dividing this by the total photon path l yields

$$\Theta^y \approx \frac{2\,l_{\text{pri}}}{l}\alpha^y - \frac{2\,l_{\text{sec}}}{l}\beta^y \approx A^y\alpha^y + B^y\beta^y \tag{2.8}$$

where the factors in front of the actual mirror tilts α^y and β^y are defined to be the magnification factors. The above equation is for illustrative purposes only and represents a simplified view because is doesn't take effects from rotations around the alternative (here z-) axis into account. The full expression used in the alignment procedure is shown in Equation 2.4.
The magnification factors are determined using a data-driven method. Eight independent calibrational rotations (positive/negative rotations about the y- / z- axis for the primary and secondary mirrors) are introduced. Then the resulting misalignment on the detector plane is measured and used to solve Equation 2.8 for the magnification factors. The final value of each magnification factor is arithmetical mean of the two corresponding values obtained with the calibrational rotations in opposite directions.
The size of each calibrational rotation for RICH1 is chosen to be ± 0.7 mrad in order to sufficiently determine the magnification factors. This choice is motivated by the fact that the Cherenkov angle resolution for RICH1 is around 1.6 mrad. Due to the smaller resolution of 0.7 mrad in RICH2, the size of its calibrational rotations is chosen to be ± 0.3 mrad.

2.3.4 Determining individual mirror misalignments

The fits to the $\delta\theta$ vs. ϕ distributions yield the misalignments in y and z on the detector plane for a given mirror combination. In order to determine the actual positioning of the mirrors for the LHCb conditions database, the misalignments of the individual primary and and secondary mirrors are needed. This gives a system with more unknowns (individual mirror misalignments in y and z) than equations. However, an optimal alignment can be achieved if each component of the optical system is properly aligned relative to all others. Therefore all mirrors only need to be aligned with respect to each other.

*** Needs to be written. ***

2.4 The Online Alignment Framework

2.4.1 Dataflow in Run II

The LHCb trigger strategies for the Run I and Run II data taking periods are shown in Figure 2.6.

In Run I the online event reconstruction was simpler and faster than the reconstruction used offline and did not include any information about the particle identification (PID). In order to have the same reconstruction online and offline as well as using the PID information in the HLT2 the data-taking strategy has been amended for Run II. As in Run I a rate of 1 MHz of events passes the level-0 trigger (L0) and is passed on to the first high level trigger stage (HLT1). There the events are partially reconstructed and accepted events are written to disk. At this stage the different alignments are run on a dedicated part of the buffered data. In case of a big shift in alignment constants the new constants are propagated to the LHCb conditions database and used in the subsequent processing of the events by the second high level trigger (HLT2).
The alignment tasks being performed on the data are - in the order they are being run - VELO alignment, tracker alignment, RICH alignment and finally muon chamber alignment. Each alignment has its own dedicated HLT1 line which collects a given number of events at the beginning of each fill (see Section 2.4.2 for the RICH lines). It has been found that ∼1 M events for RICH1 and ∼2 M events for RICH2 is sufficient to produce stable results. Once enough events have been collected the alignment is started.

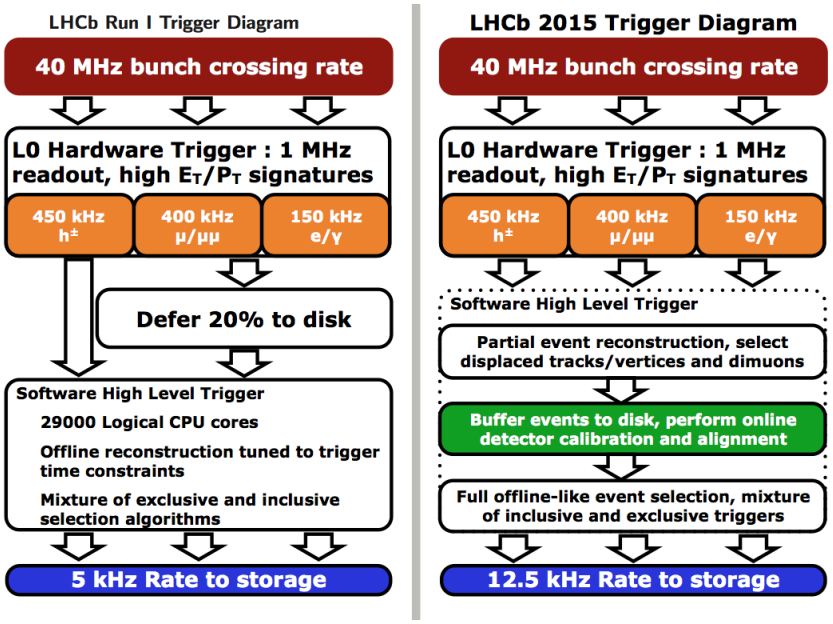

Figure 2.6: LHCb dataflow for Run I (left) and Run II (right). In Run II the data is buffered after HLT1 and an alignment is performed for each fill. The HLT2 will then process the buffered events with the updated alignment constants.

2.4.2 HLT1 selection for the RICH mirror alignment

In order to determine the misalignments on the detector plane and subsequently the individual mirror misalignments the $\delta\theta$ vs. ϕ histograms for each mirror combination have to contain enough entries for the fits described in Section 2.3.2 to converge. The minimum condition for a successful fit has been found to be that 16 of the 20 bins in ϕ have to contain at least 300 entries.
This is accomplished by having two dedicated HLT1 selections, one each for RICH1

and RICH2. The lines trigger on high energy particle tracks whose Cherenkov photons would populate the mirror combinations containing the fewest photons. The other mirror combinations are then populated by the rest of the tracks in the events.
The variables used in the selection are the track momentum p, the transverse track momentum p_T, the pseudorapidity η, the goodness of fit for the track χ^2 and the polar angle of the track ϕ. The selection criteria of tracks that are triggered upon are listed in Table 2.2.

Table 2.2: Trigger criteria for the HLT1 line for RICH1 and RICH2. Events that are accepted by these trigger lines need to have at least one track that satisfies the cuts listed below.

	RICH1	RICH2
momentum p	$p > 20$ GeV	$p > 40$ GeV
transverse momentum p_T	$p_T > 0.5$ GeV	$p_T > 0.5$ GeV
pseudorapidity η	$1.6 < \eta < 2.04$	$2.65 < \eta < 2.80$
track χ^2	$\chi^2 < 2$	$\chi^2 < 2$
polar angle Φ	$-2.65 < \Phi < -2.30$	$-2.59 < \Phi < -2.49$
	$-0.80 < \Phi < -0.50$	$-0.65 < \Phi < -0.55$
	$0.50 < \Phi < 0.80$	$0.55 < \Phi < 0.65$
	$2.30 < \Phi < 2.65$	$2.49 < \Phi < 2.59$

2.4.3 The Alignment Farm

All alignments are run on the alignment farm. The alignment farm consists of approximately 1700 CPUs, called *analysers* and a central node called the *iterator*.
The data taken from the HLT1 selection for the RICH alignments is stored evenly distributed over the analysers until it can be processed by HLT2. The analysers perform the event reconstruction with a database provided to them by the iterator and fill the $\delta\theta$ vs. ϕ histograms mentioned in Section 2.3. Apart from providing the database with the desired mirror orientations the iterator also performs the fits on the histograms, determines the individual mirror misalignments, produces a new database and decides whether the alignment procedure has converged or whether another iteration has to be performed. If the latter is the case, the iterator will make the new database available to the analysers (for more details see Section 2.4.5).
The advantage of having a system consisting of about 1700 nodes distributed over 50 farms is that the event reconstruction can happen in parallel and is therefore very fast. This parallel processing is asynchronous and has to be coordinated between the individual analysers and the iterator which is described in the next section.

2.4.4 The Control Flow

The execution of the alignment tasks is under the control of the LHCb Experiment Control System (ECS), and is implemented as a *finite state machine*, which is illustrated in Figure 2.7. The principle of a finite state machine means that each component of the system (here every individual analyser and the iterator) has to

be in one of a finite number of states at all times. The states used for the alignment procedure are also shown in Figure 2.7, such as "READY", "RUNNING" and "PAUSED". The alignment is then steered by the *run control* that can see all the components and their individual states and can send commands. Those commands will be received by the individual components and they will act accordingly. For a given state only a certain number of commands are possible - for example if the component is in state "PAUSED" it can only receive the commands "continue" and "stop". If a command is received the component will go from its state into the state declared by Figure 2.7. When in a new state the component will usually perform a task and then set itself into another state once finished so that the run control is aware of this task being completed.

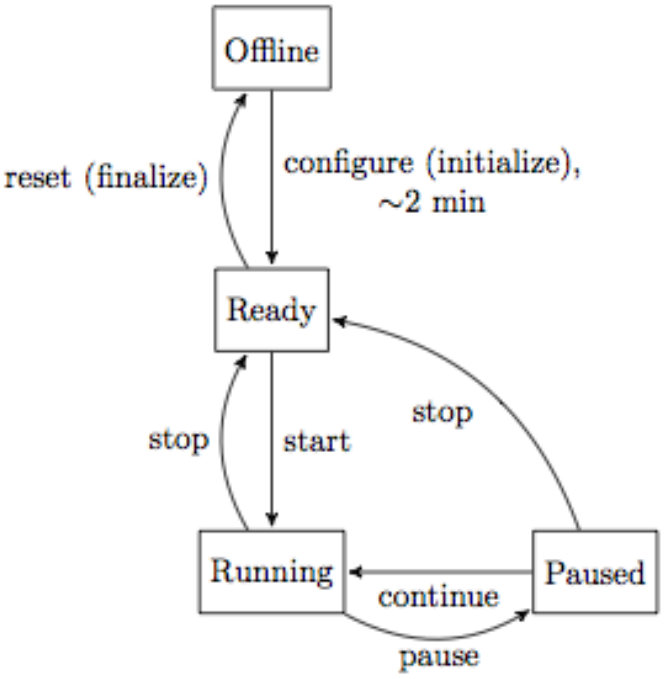

Figure 2.7: Example of one component within a system functioning under the principle of a finite state machine. The boxes show the states the component is in while the arrows show the commands the component gets from the run control.

2.4.5 Implementation of the RICH Mirror Alignment for Run II

The interplay between the iterator, one example analyser and the run control during the course of the alignment of a RICH detector is shown in Figure 2.8.
The individual analysers and the iterator all follow the same sequence of states, namely the one shown in Figure 2.7. When the alignment is being started the run control sends the command to "configure" to both the iterator and all analysers. All components will go into state "CONFIGURING" while setting up to run the alignment. For the analysers this means that they read in the configuration for the reconstruction of the events, while the iterator sets up a directory in which all files

for this alignment are saved.
Each component goes into state “READY” when it is done configuring. When all tasks are in the “READY” state, the iterator makes an initial set of alignment constants available to the analysers and then updates its state to “RUNNING”. The analyzers are then sent the“start” command, update their state to “RUNNING” and start reconstructing the data stored on them. Each analyser that has completed processing its data updates its state to “PAUSED”, and once they have all reached this state, the run control sends the âstopâ command and they update their states to “READY”. The iterator is then sent the “pause” command, collects and combines the histograms produced by the analyser tasks and performs the fits. It then calculates the individual mirror misalignments and produces a new database containing the mirror orientations. The it either indicates that conversion has been reached by updating its state to “READY”, or that further iteration is required by updating its state “RUNNING”. In the latter case the iterator will provide the new database to the analysers before changing its state and another iteration is started.

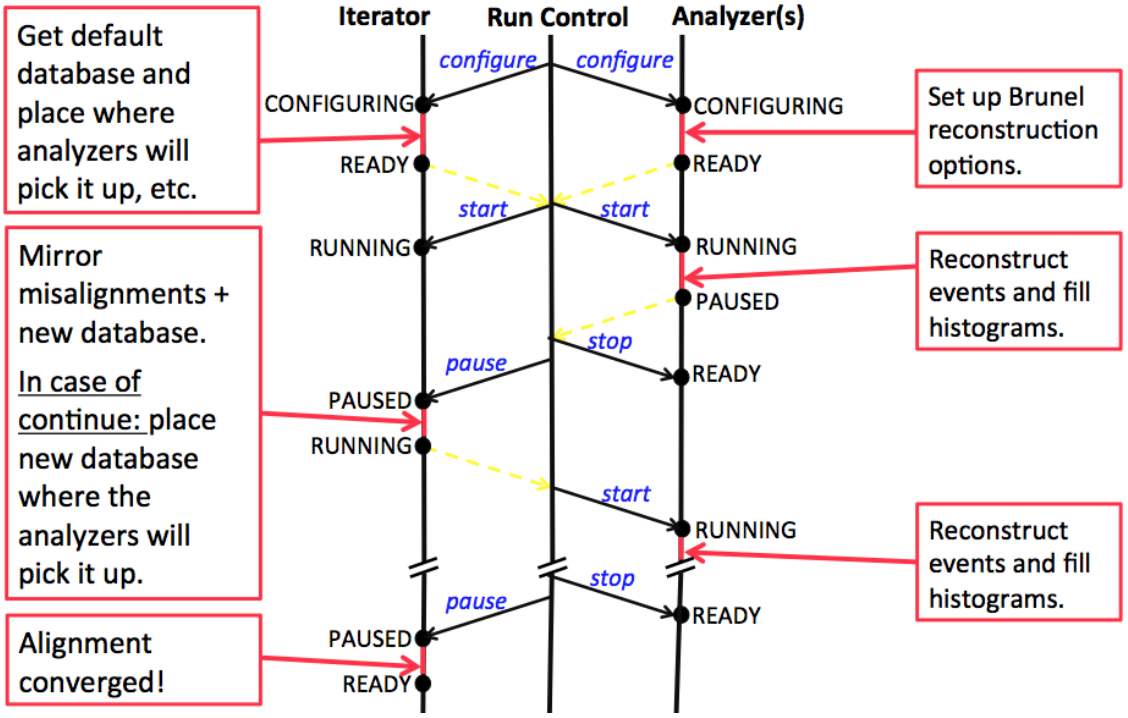

Figure 2.8: Interplay between the iterator, one example analyser and the run control during the RICH alignment procedure. The analysers reconstruct the data and produce the histograms that the iterator evaluates. The run control makes sends commands to the iterator and the analysers to make sure the alignment procedure happens in the necessary sequence.

2.5 Results

*** Results need to be summarized, chapter needs to be written. This will probably be done a bit later when more results have been generated but running automatically. ***

Future plans

3.6 Publications, talks, posters

3.6.1 Publications

First determination of the CP content of $D \to \pi^+\pi^-\pi^+\pi^-$ *and updated determination of the CP contents of* $D \to \pi^+ pi^-\pi^0$ *and* $D \to K^+K^-\pi^0$, published in Physics Letters B PLB-D-15-00624

Software framework and method for the alignment of the LHCb RICH optical system using proton-proton collisions during LHC Run II, public note being written

The novel real-time alignment and calibration of the LHCb detector, paper being written

3.6.2 Talks

RICH mirror alignment, LHCb PPTS meeting the 13/07/2015

The RICH mirror alignment, at LHCb UK 2016 meeting in Liverpool

Update on Alignment and Calibration, at LHCb week March 2016

RICH mirror alignment, LHCb PPTS meeting the 23/05/2016

Several presentations regularly given in the weekly LHCb RICH software meeting

3.6.3 Posters

Towards a model-independent measurement of γ *with* $B \to D\ K$, $D \to 4\pi$ *decays with LHCb and CLEO-c*, UK HEP December 2013

Novel Real-time Calibration and Alignment Procedure for LHCb Run II, LHCC March 2016

3.7 Future work

The work for the next year includes the following steps

- update to AlignmentOnline v11 during TS (will take half a day)
- plug my code for the monitoring together with the code written by Roel (maybe a couple of days)

- finish writing the public note about the RICH mirror alignment in Run II
- find some plots to show in my thesis about the new RICH mirror alignment to have something to show for
- be consultant for Sam working on c_i and s_i measurement
- get Sam the missing cleo-c data
- start working on the γ measurement at LHCb asap

3.8 Thesis outline

- **Chapter 1: Introduction and overview** (5 pages)

- **Chapter 2: Theory** (15 pages)
  Includes the Standard Model with a special emphasis on CP violation and the CKM matrix; Amplitude-model-independent methods to measure γ in $B \to D\ K$ decays, binned analysis measuring/using c_i and s_i and global analysis measuring/using the CP even fraction F_+.
- **Chapter 3: The LHCb Detector** (20 pages)
  LHCb detector with special emphasis on the RICH system.

- **Chapter 4: Real-time RICH alignment at LHCb** (30 pages)
  Implementation of novel, real-time RICH alignment and summary of some results.

- **Chapter 5: LHCb analysis** (30 - 40 pages)
  Measuring γ with $B \to D\ K$, $D \to 4\pi$ probably with $B \to D\ \pi$ as control sample.
- **Chapter 6: Conclusion** (5 pages)

Bibliography

[1] A. A. Alves Jr. et al. The LHCb detector at the LHC. *JINST*, 3:S08005, 2008.

[2] M. Adinolfi et al. Performance of the LHCb RICH detector at the LHC. *Eur. Phys. J.*, C73:2431, 2013.

[3] R. Aaij et al. LHCb detector performance. *Int. J. Mod. Phys.*, A30:1530022, 2015.

[4] LHCb RICH technical design report, 2000.

[5] LHCb technical design report: reoptimized detector design and performance, 2003.

[6] A. Gorisek, P. Krizan, S. Korpar, and M. Staric. Alignment of the HERA-B RICH optical system with data. *Nucl.Instrum.Meth.*, A433:408–412, 1999.

[7] A. Papanestis. The calibration and alignment of the LHCb RICH system. *Nucl.Instrum.Meth.*, A595:248–251, 2008.

[8] W. Baldini, J. Blouw, S. Blusk, N. Gilardi, O. Deschamps, et al. LHCb alignment strategy, 2006.

[9] I. Antcheva, M. Ballintijn, B. Bellenot, M. Biskup, R. Brun, et al. ROOT: A C++ framework for petabyte data storage, statistical analysis and visualization. *Comput.Phys.Commun.*, 182:1384–1385, 2011.